Available online at www.sciencedirect.com
ScienceDirect
Polymer 48 (2007) 2380–2386
polymer
www.elsevier.com/locate/polymer

Interface morphology snapshots of vertically segregated thin films of semiconducting polymer/polystyrene blends

Fernando A. Castro [a,b,*], Carlos F.O. Graeff [c], Jakob Heier [a], Roland Hany [a]

[a] Empa, Swiss Federal Laboratories for Materials Testing and Research, Laboratory for Functional Polymers, Überlandstr. 129, CH-8600 Dübendorf, Switzerland
[b] Departamento de Física e Matemática – Faculdade de Filosofia, Ciências e Letras de Ribeirão Preto – Universidade de São Paulo, Av. Bandeirantes 3900, 14040-901 Ribeirão Preto – SP, Brazil
[c] Departamento de Física, Faculdade de Ciências, UNESP, Av. Luiz Edmundo Carrijo Coube 14-01, 17033-360 Bauru, Brazil

Received 26 January 2007; received in revised form 22 February 2007; accepted 23 February 2007
Available online 28 February 2007

Abstract

We present atomic force microscopic images of the interphase morphology of vertically segregated thin films spin coated from two-component mixtures of poly[2-methoxy-5-(2′-ethylhexyloxy)-1,4-phenylene-vinylene] (MEH-PPV) and polystyrene (PS). We investigate the mechanism leading to the formation of wetting layers and lateral structures during spin coating using different PS molecular weights, solvents and blend compositions. Spinodal decomposition competes with the formation of surface enrichment layers. The spinodal wavelength as a function of PS molecular weight follows a power-law similar to bulk-like spinodal decomposition. Our experimental results indicate that length scales of interface topographical features can be adjusted from the nanometer to micrometer range. The importance of controlled arrangement of semiconducting polymers in thin film geometries for organic optoelectronic device applications is discussed.

Keywords: Polymer demixing; Polymer blends; MEH-PPV

1. Introduction

Spin-coated thin films of blends of polymers are increasingly used as the active semiconducting layer in light-emitting diodes [1–3] and photovoltaic (PV) devices [4–8]. A mixture of polymers with different electronic functionalities allows for exciton dissociation and charge recombination at donor–acceptor heterojunctions as well as more balanced electron and hole transport, fundamental processes crucial to the efficiency of these devices. Due to the low entropy of mixing, mixtures of polymers tend to phase separate [9–11]. In thin films, the substrate and vacuum surfaces have strong influence on the morphology [12–15]. In the one-phase region of polymer blends an enrichment of one of the components at the interface has been reported [16,17]. In the two-phase region, a preferential aggregation of one component at the surface [18] eventually leads to a double or triple layer structure if the system develops to thermodynamic equilibrium [19].

However, kinetic effects during spin coating may result in transient non-equilibrium morphologies frozen-in by the glass transition of one or both of the polymers [20,21]. The phase separation patterns show domain sizes ranging from nanometers to micrometers [22]. The three-dimensional morphology and surface topography of the film are dependent on a number of preparation parameters, such as solvent properties [1,3,6,8,20,23–25], rate of evaporation [4,24] and composition [2,3,21,23,26].

The morphology of the blend materials and the degree of phase separation at the nanometer scale after spin coating are important issues for the device efficiency. For PV

* Corresponding author. Departamento de Física e Matemática – FFCLRP, Universidade de São Paulo – USP, Av. Bandeirantes 3900, 14040-901 Ribeirão Preto, São Paulo, Brazil. Tel.: +55 16 3602 3858; fax: +55 16 3602 4887.
E-mail address: fcastro@aluno.ffclrp.usp.br (F.A. Castro).

0032-3861/$ - see front matter © 2007 Elsevier Ltd. All rights reserved.
doi:10.1016/j.polymer.2007.02.059

applications, the small exciton diffusion length (≤20 nm) requires the donor and acceptor materials to be in intimate contact. On the other hand, the transport of the separated charges must be ensured as well and each material must provide continuous paths for the transport of charges to their respective contacts. These requirements suggest that an optimized PV morphology consists of a hole-transporting polymer covering the anode and an electron-transporting polymer covering the cathode selectively, with a large interface between the two materials.

This idealized bilayer architecture is difficult to spin-coat from a blend of two semiconducting polymers directly. Bottlenecks and isolated domains often act as charge traps and charge recombination centers; thus, reduced carrier mobility [27,28] and increased cell series resistance [28–30] are common issues in blend heterojunction PV devices. Also, full lateral demixing during spin coating is undesired. This is because both components then contact both electrodes at the same time, resulting in a lowering of the open-circuit voltage [30].

We recently proposed to deposit the two semiconducting materials in a more controlled, two-step sequence [31]. Thereby, an immiscible hole-conducting polymer/guest polymer mixture was spin coated in a first step to produce a vertically segregated film with a highly folded interface. Subsequently, the guest material was removed using a selective solvent, and the remaining structured layer was covered with an electron-accepting material. This allowed the fabrication of efficient bilayer photovoltaic device architectures with a large interface area and selective charge transport pathways at the same time.

Here, we present in detail a series of AFM snapshots of the first step to fabricate nanostructured, hole-transporting semiconducting polymer layers. Thin films of blends of the active component poly[2-methoxy-5-(2′-ethylhexyloxy)-1,4-phenylene-vinylene] (MEH-PPV) and the guest polymer polystyrene (PS) were spin coated onto PEDOT:PSS layers, a material that is commonly used as a hole-injection and buffer layer on top of the ITO anode in PV devices. PS was then dissolved with the selective solvent cyclohexane, and the remaining MEH-PPV layer topographies were examined with atomic force microscopy. We demonstrate the developing morphologies for different solvents, compositions and polystyrene molecular weights, and discuss characteristic parameters that control the polymer-based self-organization process.

2. Experimental

Mica (1×1 cm^2) was used as substrate, on which an 80 nm thick layer of poly(ethylene dioxythiophene) doped with polystyrene sulfonic acid (PEDOT:PSS, Bayer) was spin coated. After drying under vacuum, the substrates were transferred to a nitrogen-filled glove box (<1 ppm O_2 and H_2O). MEH-PPV ($M_n \sim 47\,000$, Aldrich) was purified by dissolving in THF (1 g/100 ml), followed by filtration, precipitation in a 10-fold excess of methanol and drying in a vacuum oven at 65 °C. Stock solutions of MEH-PPV (5 mg ml^{-1}) and polystyrene (10 mg ml^{-1}, PS GPC standards from Fluka with molecular weights of $M_w = 3000$, 10 000, 70 000, 150 000 and 230 000, referred to as PS3K, PS10K, PS70K, PS150K and PS230K, respectively) were prepared in chlorobenzene and mixtures of chloroform and chlorobenzene. Blended films were prepared by mixing together different quantities of MEH-PPV and PS stock solutions before spin coating. The spin rotation parameters were kept constant (acceleration to 3000 rounds per minute in 6 s, constant 3000 rounds per minute for 1.5 min). If necessary, the blend solution was diluted to adjust the final average MEH-PPV film thickness to 30–40 nm, corresponding to an absorbance of ∼0.25 at 515 nm. PS was then removed by dipping the substrate for 1 min into the selective solvent, cyclohexane. Atomic force microscopic (AFM) measurements were performed on a Digital Instruments Multimode Scanning Microscope (Nanoscope III) or on a Nanosurf Mobile S in tapping mode at a resonance frequency of 325 kHz or 170 kHz, respectively. We used rectangular silicon cantilevers (Mikromasch, Nanosensors™) with a typical force constant of ∼40 N/m and a tip radius of curvature of ∼10 nm. Dissolution of PS from blended films was investigated with a UV–vis spectrophotometer (Varian Cary 50, 1.5 nm spectral bandwidth, scan rate 600 nm min^{-1}). As a baseline, we used a clean quartz substrate over which an 80 nm thick PEDOT:PSS layer was deposited. Blend solutions of MEH-PPV and PS were then spin coated on the same substrate, and films were kept in cyclohexane for 1 min. The decrease of the absorption in the 200–250 nm range was used to confirm the complete dissolution of PS, and the constant absorbance in the 400–600 nm range showed that MEH-PPV was not affected by the solvent. In order to confirm that the topography was not simply formed or distorted by the solvent used for PS removal, we investigated the surface of MEH-PPV-only films after dipping in cyclohexane from a few seconds to 10 min (data not shown). No surface modification or swelling was observed. Comparable AFM images were obtained after storing samples in the glove box for several weeks, indicating the stability of topographical features in these films.

3. Results and discussion

Our analysis of the samples is restricted to the ‘‘frozen-in’’ phase morphology after spin coating has been completed. As we have no capabilities to monitor the kinetics of the spin coating in detail, information on the film formation process has to be inferred from the finally obtained non-equilibrium structures. The spin-coating process is described as a quench by solvent extraction. Different from a temperature quench, phase separation during a quench by solvent extraction is rather complex and involves several hydrodynamic regimes and diffusive processes [32]. Many parameters inherent to the experimental system, such as viscosities, surface and interfacial tensions change continuously.

We start by looking at the top surfaces of as spin-coated blend films (Fig. 1). These surfaces are flat on a 10-nm scale. This observation is unusual for strongly interacting polymer blend systems spin coated from solution, which normally show free surface undulations [20,21] depending on the ratio

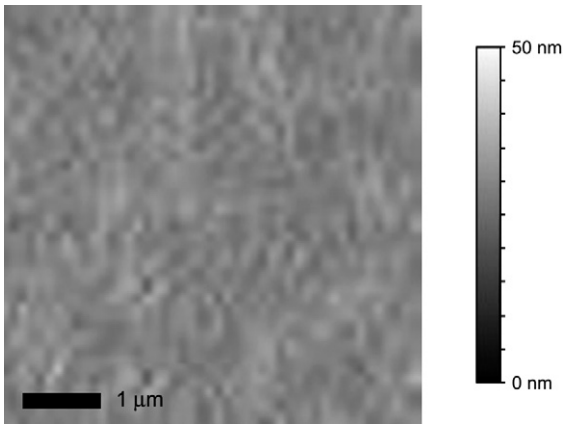

Fig. 1. AFM image of an as spin-coated film using a 1:2 w/w blend solution of MEH-PPV/PS150K in chlorobenzene.

of the interfacial tension between the different phases and the surface tension against the vacuum interface [33]. In addition, spin-coating blends with large differences in the solubility of the individual polymers in the common solvent can lead to marked height differences between the different phases. One of the phases will solidify first followed by a collapse of the second phase. We explain the relative smoothness of the MEH-PPV/PS blend films with the similarity of the solubility parameters of MEH-PPV and PS. The values given for MEH-PPV range from $\delta = 9.96\ \mathrm{cal}^{1/2}\,\mathrm{cm}^{-3/2}$ to $8.9\ \mathrm{cal}^{1/2}\,\mathrm{cm}^{-3/2}$ [34,35]. The solubility parameter of PS is consistently reported to be $\delta = 9.1\ \mathrm{cal}^{1/2}\,\mathrm{cm}^{-3/2}$. With the solubility parameters of chloroform ($\delta = 9.21\ \mathrm{cal}^{1/2}\,\mathrm{cm}^{-3/2}$) and chlorobenzene ($\delta = 9.15\ \mathrm{cal}^{1/2}\,\mathrm{cm}^{-3/2}$) [36], we also conclude that both, chloroform and chlorobenzene, are slightly better solvents for PS.

In Fig. 2, we show the phase structures of different MEH-PPV/PS blend films after removal of the PS phase. For the high molecular weight mixtures (M_w(PS) = 70k, 150k and 230k), a pronounced lateral phase separation structure and features with a height exceeding ~100 nm dominate the film morphology, while for the low-molecular weight mixtures (PS3K and PS10K), a bilayer structure is established with a rather smooth interface (maximum topographical feature ~10 nm). For the high molecular weight PS polymer blends "bulk-like" spinodal decomposition seems to dominate over the formation of a wetting layer, while for lower molecular weight polystyrenes it is the other way around.

We describe the film morphology formation process with the help of a schematic diagram (Fig. 3). A detailed description of how a solvent quench experiment compares to a temperature quench has been given by Dalnoki-Veress et al. [37].

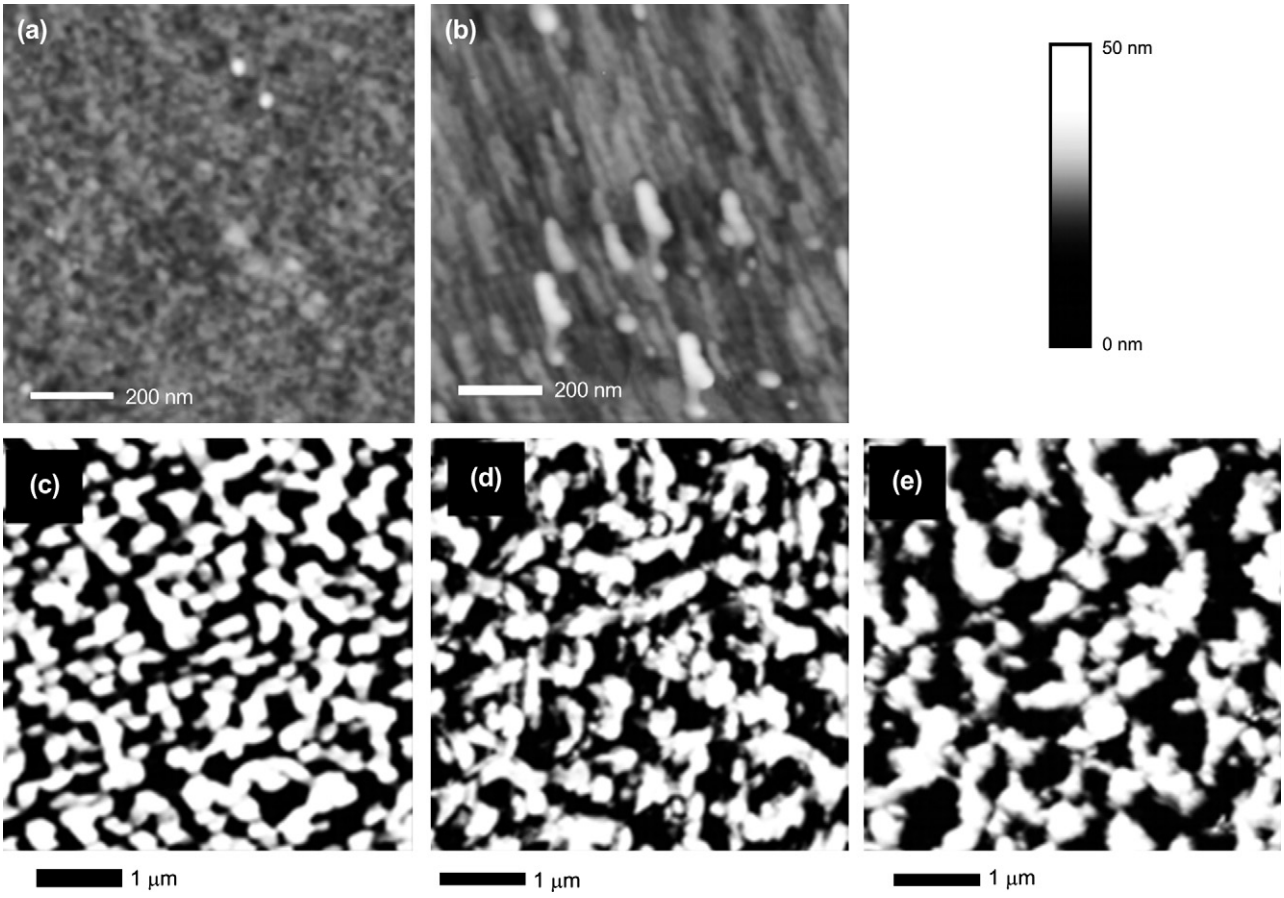

Fig. 2. AFM images of structured MEH-PPV films after polystyrene (PS) removal. Films were spin coated from MEH-PPV/PS (1:2 w/w) blends in a 1:1 vol/vol solvent mixture of chlorobenzene and chloroform. AFM scans are shown for different molecular weights of PS: (a) M_w (PS) = 3000 (PS3K), (b) PS10K, (c) PS70K, (d) PS150K, and (e) PS230K.

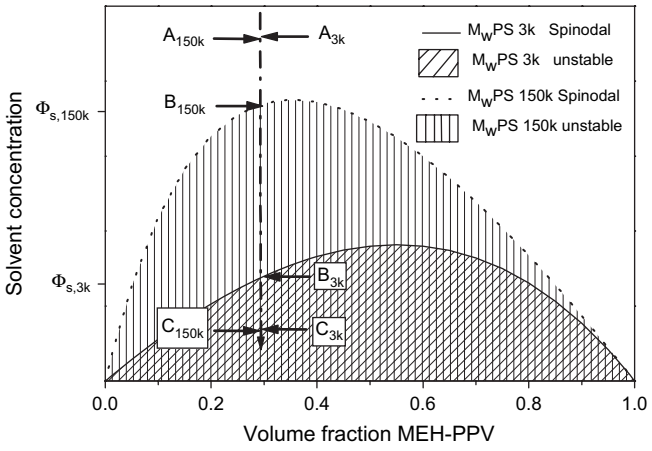

Fig. 3. Schematic bulk-phase diagram of a polymer/polymer/solvent system for two different molecular weights. The diagram does not account for the influence of wetting on the shape of the spinodal. During the solvent quench, enrichment layers form at the surfaces (A) before entering the unstable region (spinodal, B). The morphology will be frozen at the glass transition of the polymers (C). While the formation of surface enrichment layers and the glass transition is quasi independent of molecular weight, the spinodal line depends strongly on molecular weight.

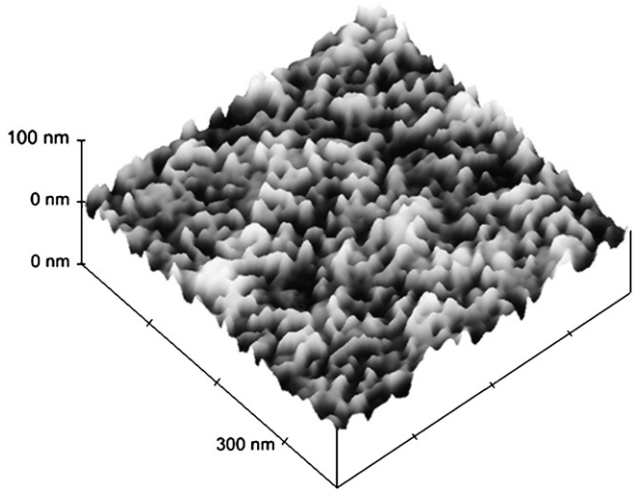

Fig. 4. AFM image of a MEH-PPV surface after removal of the PS phase. The film was spin coated from a MEH-PPV/PS3K (1:2 w/w) mixture in chlorobenzene. The Fourier transform of this surface shows a peak at 166 nm due to spinodal structures in analogy with Fig. 2b–e. In addition, a plateau at smaller wavelengths (~27 nm) corresponds to the visible substructures with dimensions well below 100 nm.

During spin coating, a layer is formed on the substrate which subsequently thins due to fluid flow and evaporation [38,39]. The phase morphology and its time evolution are governed by an interplay between two phenomena: first, the preferential interaction of MEH-PPV with the polar PEDOT:PPS layer and PS with the vacuum surface leads to the formation of enrichment layers (A, Fig. 3) of MEH-PPV against the substrate and of PS against the vacuum surface; second, below solvent concentrations Φ_s, phase separation between the two components starts from the mixture that presumably exists in solution (B, Fig. 3). The bulk-phase diagram also indicates the influence of the molecular weight on the phase behaviour. The high molecular weight PS blends have a higher effective interaction parameter, resulting in ''early'' phase separation, whereas for low-molecular weight PS, the phase separation process effectively starts from a higher polymer concentration.

Our experimental observations suggest the following structure formation process: for the high molecular weight PS blends, bulk-like phase separation sets in from solution, favouring one spinodal wavelength. The influence of the surfaces on this process may be rather small. The spinodal pattern of this process will be frozen-in during the final rapid solvent quench and will collapse onto the substrate (Fig. 2c–e). For the low-molecular weight blends, phase separation only starts at a lower solvent concentration, which implies that the film is thinner and the influence of the interfaces on the phase separation kinetics is more pronounced. In that case, enrichment layers are formed that stabilize an interface running parallel to the surfaces (Fig. 2a and b). However, a higher lateral resolution AFM image also reveals less pronounced spinodal patterns at the interface for low-molecular weight PS samples (Fig. 4).

Note that Fig. 3 represents a snapshot of the very early stages of the spin-coating process and does not account for the influence of wetting. For a thinning film the interface potential will influence the shape of the bulk-phase diagram. During the solvent quench we thus expect a continuous change in the shape of the spinodal lines. Depending on film thickness and interfacial interactions, eventually wetting transitions, capillary condensation or interface localization/delocalization takes place [40]. These effects may only be observed by resolving the full dynamics of the spin-coating process.

In the following, we substantiate the claim that bulk spinodal decomposition is the dominant mechanism driving the phase separation for MEH-PPV and PS. Fig. 5a shows the Fourier transform analysis of the topographical image shown in Fig. 2c; a ring typical for a spinodal process is clearly visible. Fig. 5b shows a log–log plot of the characteristic wavelengths as a function of the arithmetical mean of the degrees of polymerization, extracted from the power spectra of the AFM scans. If PS3K is excluded from the analysis, the data follows a scaling law with critical exponents 0.54 ± 0.06 and 0.46 ± 0.14 for samples spin coated from a mixture of chlorobenzene and chloroform, and of chlorobenzene only. The exponents were obtained by a linear regression analysis of the peak wavelength in the power spectral density. The peak wavelength values have not been weighted with the individual error bars, because they do not represent a scatter in data but the width of the power spectral density. The values for the scaling exponents compare well with the molecular weight dependence of the correlation length of concentration fluctuations (ξ) in a bulk sample [11,41]. ξ is given by $\xi \sim$ (degree of polymerization $N)^{0.5}$ for a symmetrical polymer blend with $N = N_A = N_B$. During a solvent quench, phase separation does not occur at a fixed point in the phase diagram, but rather along a line of decreasing solvent concentration. This would imply a continuously changing correlation length, in contrast to the occurrence of one preferred wavelength we observe.

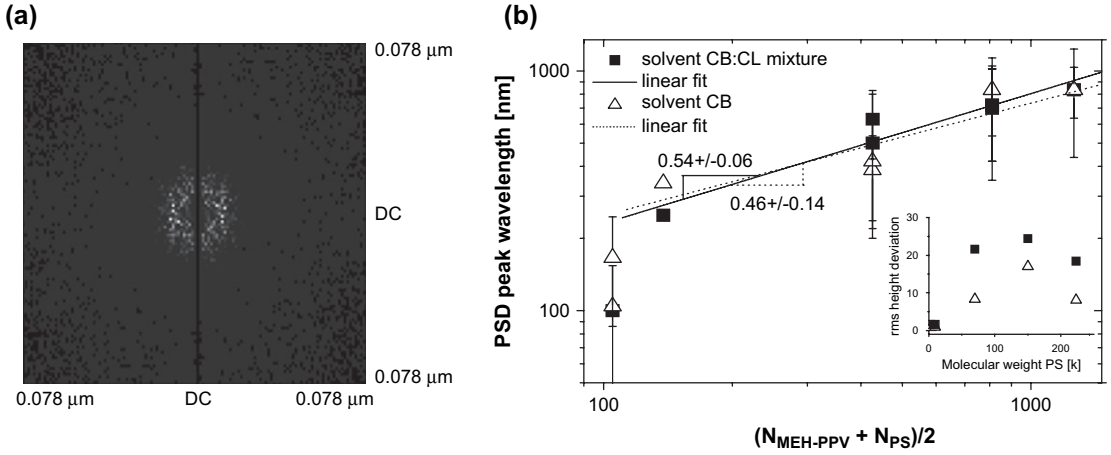

Fig. 5. (a) Numerical Fourier transform analysis pattern of the interface topographical MEH-PPV structure shown in Fig. 2c. (b) Double-logarithmic plot of the spinodal wavelengths of MEH-PPV surfaces after removal of PS, determined from the power spectra vs the mean of the degrees of polymerization. Films were spin coated from 1:2 w/w MEH-PPV/PS blends from a mixture (1:1 vol/vol) of chlorobenzene (CB) and chloroform (CL), and of CB only. Linear fits are plotted independently for two different datasets (solvents). The linear fit was performed excluding the two PS3K samples. The error bars indicate the wavelength where the two-dimensional isotropic power spectral density (PSD) peak dropped to one half. The inset of Fig. 5b shows root-mean-square (rms) height deviations extracted from the AFM scans for MEH-PPV phase patterns as a function of PS molecular weight.

We suggest this to be the signature of the rapid solvent quench during spin coating. In addition, the wavelengths may establish at different relative positions in the phase diagram for samples with different molecular weights, leading to a vaguely defined scaling exponent. This effect seems not to be predominating and we observe a molecular scaling behaviour.

There is not a large difference in the spinodal patterns in films casted from solutions with different solvent compositions and the dominant wavelength of the features is the same (within the experimental error). The inset of Fig. 5b displays the resulting MEH-PPV feature heights using different PS molecular weights for the two different solutions. The vapour pressure of chloroform is 197 mm Hg at 25 °C, whereas the vapour pressure of chlorobenzene is only 12 mm Hg [42]. Chloroform is thus a much faster evaporating solvent. In a mixture of chloroform and chlorobenzene, the early stages of solvent evaporation should be governed by the evaporation rate of chloroform, while for the later stages the evaporation rate of chlorobenzene is rate determining. The amplitude of the features is higher for samples spin coated from a solvent with a higher chloroform volume fraction. The roughness maximum was found at a PS molecular weight of 150k. The conservation of the spinodal wavelength supports our hypothesis that due to the overall rapid solvent quench, spinodal decomposition occurs at one wavelength only and coarsening does not occur. The observation that the amplitude of the features is higher when a chlorobenzene/chloroform mixture is used as a solvent is in marked contrast to most observations where a fast evaporating solvent does not allow for the development of a spinodal decomposition pattern at all [24,25]. In our case, the very fast initial evaporation rate of chloroform may hinder the formation of a substantial enrichment layer thereby emphasizing the lateral spinodal pattern. We indeed observe a slight decrease of the wetting layer thickness.

For photovoltaic applications the most interesting phase morphology is where (a) a MEH-PPV wetting layer is fully established at the PEDOT:PSS/ITO/glass surface and (b) the length scales of the topographical patterns are below 100 nm. Both of these requirements could be observed in blends of MEH-PPV and PS of molecular weight $M_w = 3000$. From the log–log plot shown in Fig. 5b, we also conclude that a different/additional mechanism may be responsible for the structure formation using PS3K. Some of these samples indeed show substructures on smaller length scales (Figs. 4 and 6). We thus investigated in more detail the influence of the solvent and weight fraction of PS on the characteristic surface roughness in the remaining MEH-PPV layer for these blends.

Surfaces were characterized by measuring the root-mean-square (rms) surface roughness and the maximum valley to peak heights (R_t, Table 1). The following trends were observed: first, the surface roughness increases with an increasing fraction of chloroform, even though the differences are not

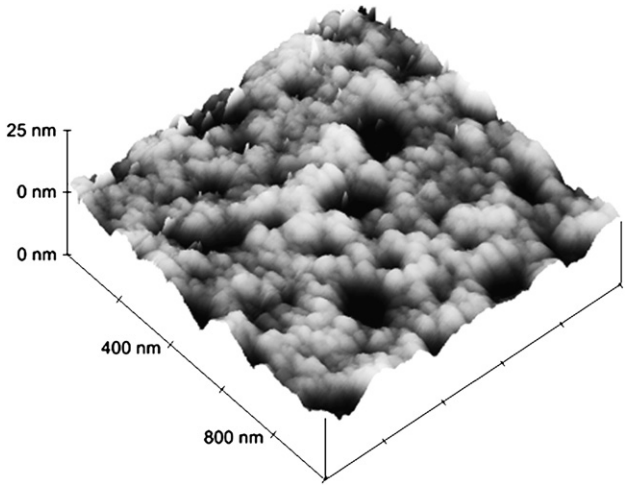

Fig. 6. AFM scan of a MEH-PPV surface after removal of PS. The film was spin coated from a MEH-PPV/PS3K (1:1 w/w) mixture dissolved in chloroform.

Table 1
Root-mean-square surface roughness (rms) taken from the mean data plane, and the maximum vertical distance (R_t) between the lowest and highest data point in the AFM image

Solvent [vol/vol]	Blend composition MEH-PPV/PS [w/w]			
	1:1	1:2	1:3	1:4
	rms [nm]/R_t [nm]			
CB	1.2/22.1	0.9/6.1		
CB:CL = 2:1	1.6/14.3			
CB:CL = 1:1	1.0/11.9	1.1/8.5	0.8/6.0	2.1/31.1
CB:CL = 1:2	1.0/8.3		1.4/19.0	
CB:CL = 1:3		1.8/33.7		
CB:CL = 1:5			1.6/22.5	
CL	2.1/15.8			

MEH-PPV/PS ($M_w = 3000$) blends of different compositions spin coated from various solvent mixtures (CB = chlorobenzene, CL = chloroform) were investigated after removal of polystyrene.

very distinct (the same has been observed for the higher molecular weight mixtures). The greatest roughness results when pure chloroform is used as the solvent (Fig. 6). This is explained with our model as described earlier: the evaporation rate of chloroform is so fast that now even for the low-molecular PS no enrichment layer can be established. Second, the rms values also indicate a slight increase for increasing PS weight fractions in the blend, possibly due to an increase of the bulk correlation length for higher PS content; for larger wavelengths, the interfacial tension allows for larger amplitudes. The maximum peak-to-valley distances R_t given in Table 1 are not average values, but are useful to detect extreme topographical features, such as small cracks or pinholes associated with short circuit problems in optoelectronic thin film device applications.

Another model proposes that phase separation in thin films only proceeds via the instability of polymer interfaces that form parallel to the film surfaces rather than bulk-like composition fluctuations [32,43]. The origin of this instability can be manifold, ranging from dewetting instabilities over polymer–solvent demixing to convection instabilities caused by rapidly evaporating solvents. The latter process will be more pronounced for fast evaporating solvents, whereas for solvents with low evaporation rates, diffusion of the solvent through the film is more likely able to maintain a spatially uniform solvent concentration, decreasing the driving force for the interfacial instability [44]. Potentially, the interface between the stratified layers then becomes unstable due to Marangoni convection (evaporation causes cooling at the interface), leading to the final lateral phase-separated thin film structures. De Gennes [45] and Birnie [46] have pointed out that during the spin-coating process the concentration effects (solutocapillary) are more important than the temperature gradient (thermocapillary).

Recently, Jones and co-workers have developed a technique to monitor the dynamics of the spin-coating process and the development of phase-separated structures in situ as it happens, confirming the formation of a transient bilayer structure in their system [38,44]. Our observations do not support this scenario for blend mixtures of high molecular weight. Inherent to all convection instabilities is an initial capillary wave whose wavelength is independent of molecular weight [47,48]. The wavelength only becomes molecular weight dependent in a later stage of the structure development. Once a capillary wave is established, it is the viscosity that determines an increase in wavelength. As explained earlier, due to the speed of the solvent quench, we do not believe that coarsening plays a significant role in our system.

We described the mechanisms in thin films of polymer blends leading to the final interface textures as observed here. We anticipate that the structure formation process is governed by spinodal decomposition. The spinodal wavelength as a function of the molecular weight of PS follows a scaling law with the exponent $\alpha \sim (0.50 \pm 0.04)$. These sub-micron structures are easily reproduced and can be ''controlled'' by adjusting the experimental parameters. In particular, variation of the molecular weight of the guest polymer provides a powerful tool to optimize the interface structure. Higher molecular weights of the guest polymer increase the feature amplitudes and wavelengths of the spinodal pattern. Fine tuning can be done by selecting an optimized solvent and mixing ratio of the polymer blend.

From an application point of view, we are able to produce nanostructured MEH-PPV layers with different characteristic surface features that can be used as active electron-donor layers in solar cells. The performance and stability of real devices were tested after depositing the electron-acceptor C_{60} fullerene on top of the MEH-PPV layer [31]. Results indicated that the nanostructure is stable at the relevant temperature in a working solar cell. From that investigation we could relate the efficiency of the solar cells to their internal morphology. The nanostructured cells resulted in much-improved device performance, with external power efficiencies of $\sim$0.6% for white light and $\sim$3% for monochromatic illumination at 500 nm. These values are more than 3 times higher than those reported for that particular material combination so far [31].

4. Conclusion

This work demonstrates a versatile method for the fabrication of nanostructured layers of semiconducting polymers and provides some insight into the experimental spin-coating conditions that allow tuning the resulting topographical length scales from the nanometer to micrometer range. The substantial freedom in the choice of the guest polymer leads one to suppose that the procedure is not restricted to the MEH-PPV component. Rather, it may be applicable to other popular semiconducting polymers, such as poly(3-hexylthiophene), as well. The proposed two-step concept for controlling the heterointerface in organic optoelectronic devices allows for the independent adjustment of the desired topography of the first layer (as demonstrated here) that can be covered by a series of second active components. This offers a great flexibility to balance exciton dissociation and charge transport requirements in photovoltaic and light-emitting diode applications, and adds a variant of a processing route for the controlled design of optimum device performance.

Acknowledgments

We acknowledge funding from COST (Coopération européenne dans le domaine de la recherché scientifique et technique) and from FAPESP (Brazil), and thank B. Sinnet (EAWAG) for the use of the Nanoscope III and J. Groenewold (Delft) for helpful discussions.

References

[1] Corcoran N, Arias AC, Kim JS, MacKenzie JD, Friend RH. Appl Phys Lett 2003;82:299.
[2] Iyengar NA, Harrison B, Duran RS, Schanze KS, Reynolds JR. Macromolecules 2003;36:8978.
[3] Voigt M, Chappell J, Rowson T, Cadby A, Geoghegan M, Jones RAL, et al. Org Electron 2005;6:35.
[4] Halls JJM, Arias AC, MacKenzie JD, Wu W, Inbasekaran M, Woo EP, et al. Adv Mater 2000;12:498.
[5] Snaith HJ, Friend RH. Thin Solid Films 2004;451–452:567.
[6] Arias AC, Corcoran N, Banach M, Friend RH, MacKenzie JD, Huck WTS. Appl Phys Lett 2002;80:1695.
[7] Halls JJM, Walsh CA, Greenham NC, Marseglia EA, Friend RH, Moratti SC, et al. Nature 1995;376:498.
[8] Arias AC. J Macromol Sci Polym Rev 2006;46:103.
[9] De Gennes PG. J Chem Phys 1980;72:4756.
[10] Pincus P. J Chem Phys 1981;75:1996.
[11] Binder K. J Chem Phys 1983;79:6387.
[12] Reich S, Cohen Y. J Polym Sci B 1981;19:1255.
[13] Lipatov YS, Nesterov AE, Ignatova TD, Gudima NP, Gritsenko OT. Eur Polym J 1986;22:83.
[14] Budkowski A. Adv Polym Sci 1999;148:1.
[15] Geoghegan M, Krausch G. Prog Polym Sci 2003;28:261.
[16] Nakanishi H, Pincus P. J Chem Phys 1983;79:997.
[17] Schmidt I, Binder K. J Phys 1985;46:1631.
[18] Jones RAL, Norton LJ, Kramer EJ, Bates FS, Wiltzius P. Phys Rev Lett 1991;66:1326.
[19] Bruder F, Brenn R. Phys Rev Lett 1992;69:624.
[20] Walheim S, Böltau M, Mlynek J, Krausch G, Steiner U. Macromolecules 1997;30:4995.
[21] Walheim S, Ramstein M, Steiner U. Langmuir 1999;15:4828.
[22] Chappell J, Lidzey DG, Jukes PC, Higgins AM, Thompson RL, O'Connor S, et al. Nat Mater 2003;2:616.
[23] Li Y, Yang Y, Yu F, Dong L. J Polym Sci B 2006;44:9.
[24] Arias AC, MacKenzie JD, Stevenson R, Halls JJM, Inbasekaran M, Woo EP, et al. Macromolecules 2001;34:6005.
[25] Higgins AM, Martin SJ, Thompson RL, Chappell J, Voigt M, Lidzey DG, et al. J Phys Condens Matter 2005;17:1319.
[26] Müller-Buschbaum P, Gutmann JS, Stamm M. Macromolecules 2000;33:4886.
[27] Xue J, Rand BP, Uchida S, Forrest SR. Adv Mater 2005;17:66.
[28] Peumans P, Yakimov A, Forrest SR. J Appl Phys 2003;93:3693.
[29] Yang F, Shtein M, Forrest SR. Nat Mater 2005;4:37.
[30] Snaith HJ, Greenham NC, Friend RH. Adv Mater 2004;16:1640.
[31] Castro FA, Benmansour H, Graeff CFO, Nüesch F, Tutis E, Hany R. Chem Mater 2006;18:5504.
[32] Sprenger M, Walheim S, Budkowski A, Steiner U. Interface Sci 2003;11:225.
[33] Müller M. Comput Phys Commun 2002;147:292.
[34] Chou HL, Lin KF, Wang DC. J Polym Res 2006;13:79.
[35] Cossiello RF, Akcelrud L, Atvars TDZ. J Braz Chem Soc 2005;16:74.
[36] Barton AFM. Handbook of solubility parameters and other cohesion parameters. Boca Raton, Florida: CRC Press, Inc.; 1983.
[37] Dalnoki-Veress K, Forrest JA, Stevens JR, Dutcher JR. J Polym Sci B 1996;34:3017.
[38] Jukes PC, Heriot SY, Sharp JS, Jones RAL. Macromolecules 2005; 38:2030.
[39] Müller-Buschbaum P, Bauer E, Wunnicke O, Stamm M. J Phys Condens Matter 2005;17:S363.
[40] Müller M, Binder K. J Phys Condens Matter 2005;17:S333.
[41] Müller M, Binder K. Macromolecules 1998;31:8323.
[42] CRC handbook of chemistry and physics. 86th ed. CRC press, Inc.; 2005–2006.
[43] Ton-That C, Shard AG, Teare DOH, Bradley RH. Polymer 2001;42: 1121.
[44] Heriot SY, Jones RAL. Nat Mater 2005;4:782.
[45] De Gennes PG. Eur Phys J E 2001;6:421.
[46] Birnie III DP. J Mater Res 2001;16:1145.
[47] Sferrazza M, Heppenstall-Butler M, Cubitt R, Bucknall D, Webster J, Jones RAL. Phys Rev Lett 1998;81:5173.
[48] Brochard-Wyart F, Martin P, Redon C. Langmuir 1993;9:3682.